Tomographic analysis of jammed ellipsoid packings

Fabian M. Schaller, Max Neudecker, Mohammad Saadatfar, Gary Delaney, Klaus Mecke, Gerd E. Schröder-Turk , and Matthias Schröter

Citation: AIP Conference Proceedings **1542**, 377 (2013); doi: 10.1063/1.4811946

View online: http://dx.doi.org/10.1063/1.4811946

View Table of Contents: http://scitation.aip.org/content/aip/proceeding/aipcp/1542?ver=pdfcov

Published by the AIP Publishing

Tomographic Analysis of Jammed Ellipsoid Packings

Fabian M. Schaller[*,†], Max Neudecker[†], Mohammad Saadatfar[**], Gary Delaney[‡], Klaus Mecke[*], Gerd E. Schröder-Turk[*] and Matthias Schröter[†]

[*]*Institut für theoretische Physik, Friedrich-Alexander-Universität Erlangen-Nürnberg, Erlangen, Germany*
[†]*Max-Planck-Institut für Dynamik und Selbstorganisation, Göttingen, Germany*
[**]*Applied Maths, RSPhysSE, The Australian National University, Australia*
[‡]*CSIRO Mathematics, Informatics and Statistics, Clayton South, Victoria, Australia*

Abstract. Disordered packings of ellipsoidal particles are an important model for disordered granular matter. Here we report a way to determine the average contact number of ellipsoid packings from tomographic analysis. Tomographic images of jammed ellipsoid packings prepared by vertical shaking of loose configurations are recorded and the positions and orientations of the ellipsoids are reconstructed. The average contact number can be extracted from a contact number scaling (CNS) function. The size of the particles, that may vary due to production inaccuracies, can also be determined by this method.

Keywords: Granular matter, Ellipsoids, Tomography, Contact numbers
PACS: 45.70.-n, 45.70.Cc, 61.43.-j, 81.70.Tx

INTRODUCTION

Random packings of spheres are the subject of much past and ongoing research [1], in particular with respect to the existence and nature of the random close packing transition. Packings of ellipsoidal particles are an obvious generalization of the sphere packing problem, with interesting properties [2, 3, 4, 5], and open questions; for example, the nature of the random close packing transition (which for spheres coincides with the onset of crystallization [6, 7, 8]) may be more complex due to the possibility of partial order, positional or orientational, as is for example the case in nematic liquid crystalline phases. X-ray tomography provides access to the 3D internal structure of experimental random packings; comprehensive studies have been performed for packings of spheres [9] and tetrahedra [10]. A simple order metric of granular packings is the average contact number, i.e. the average number of neighbors in contact with an object. As any interaction and force is transmitted from particle to particle through mutual contacts, the contact number is conceptually important for the mechanical stability of a packing. Therefore, the contact number of jammed ensembles is a well-studied parameter in the literature [11, 12, 4, 10, 9]. Due to limited resolution in experimental data the contact number is difficult to extract.

Tomography and Image Processing

Packings of ellipsoidal particles are imaged by X-Ray tomography, and a 3D raster graphics grayscale image is reconstructed from the projections (using the software phoenix datos|x - reconstruction) resulting in an image with a resolution of 0.064 mm/voxel.

FIGURE 1. (left) Loose jammed packings of frictional ellipsoidal gypsum particles ($5.3 \times 6.6 \times 6.6$ mm) produced with a 3D printer are prepared in a cylindrical container with a diameter of 104 mm. By periodic vertical tapping of the container, the packing can be further compactified. With this method packings of different packing fraction can be prepared by variation of the number of taps. (right) Detected particles after imaging by X-Ray tomography and reconstruction.

Most structural analyses of the grain packs, including the contact number analysis, require a representation of the tomographic data where the individual particles have been identified and given a unique label. This is here achieved by a watershed algorithm (similar to the description in [13]) combined with spatially variable threshold segmentation. A flow chart and an illustration of the steps of the algorithm are provided in Fig. 2.

For the particle detection algorithm a binary image is created by threshold segmentation with a radially varying segmentation threshold because in the reconstructed grayscale images a lower intensity in the center of the container and overexposures at the sides of the container

Powders and Grains 2013
AIP Conf. Proc. 1542, 377-380 (2013); doi: 10.1063/1.4811946

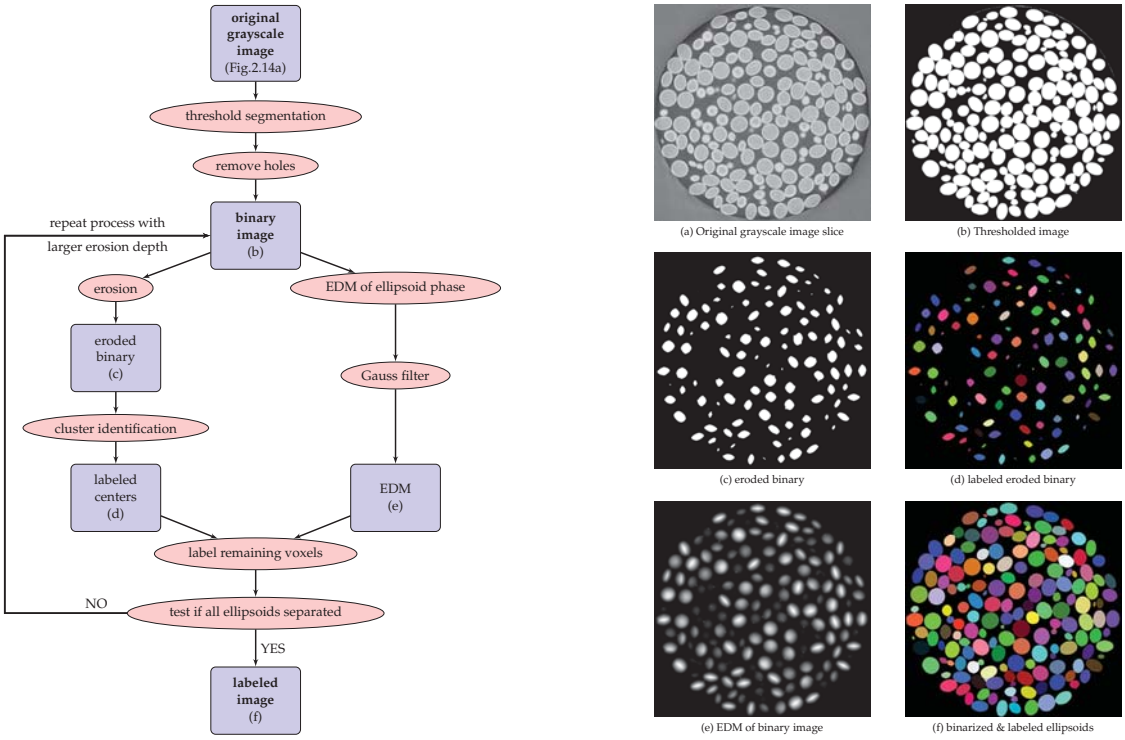

FIGURE 2. Flow diagram of segmentation algorithm. Elliptical nodes describe the segmentation steps and rectangular ones resulting data/images types. Examples of the different intermediate steps are shown on the right.

are commonly observed. The rotational symmetry of the cylindrical container means that the intensity variation is radially dependent.

By convention, we will refer to voxels representing the particles as "white" and to those representing the void space as "black".

Within the white ellipsoids of the binary image, often some spurious black voxels remain. For the separation process described below, these wrongly identified voxels have to be eliminated. To remove these holes, the Hoshen Kopelmann cluster identification algorithm [14] is used to identify all black clusters. The biggest cluster is the real air phase surrounding the particles and stays black. All the other small clusters are set to white because they are assumed to represent falsely identified black voxels, which can be caused, for example, by air bubbles in the particles or experimental noise.

After the creation of the binary image, the actual identification of the ellipsoids begins. First, the white phase (ellipsoid phase) of the image is eroded [15] by a suitably chosen erosion depth such the ellipsoids are separated (that is, each ellipsoid is represented by a unique cluster of white voxels), see below for the choice of the erosion depth. A very effective method to calculate the eroded image, is by thresholding the Euclidean distance map (EDM) of the ellipsoid phase [16]. The EDM of the white phase of a binary image labels each voxel with the distance to the nearest black voxel. It can be calculated effectively by solving a minimization problem [17].

After the erosion step, all ellipsoids are separated, as shown in Fig. 2c. The remaining parts can again be labeled and counted with the Hoshen Kopelmann algorithm [14], see Fig. 2d. The number of clusters of the eroded image is the number of ellipsoids in the analyzed part of the cylinder.

The voxels, which were previously eroded, also need to be labeled. For this step an EDM of the original binary image is needed, see Fig. 2e. To avoid unwanted artifacts in the next step, the EDM is smoothed by a Gauss filter. All white (ellipsoid) voxels that are not yet labeled (those that were eroded in the previous step) are now connected to the neighboring voxel, indicated by the gradient of the EDM. Now the connections are resolved: If a voxel is already labeled, all connected voxels are labeled equivalently. White voxels that remain unlabeled after this step are ignored: they are treated as wrongly identified white voxels that do not belong to an ellipsoid (these wrongly identified white voxels must represent clusters that are significantly smaller than the clusters representing the ellipsoidal particles).

Every cluster should represent one ellipsoid and hence all clusters should have approximately the same size in

the end, corresponding roughly to the small degree of polydispersity of the particles. Variations in cluster size that are larger than what is compatible with the particle polydispersity are an indication that some ellipsoids have not been separated by the erosion process and hence of a too small erosion depth. In this case the segmentation process is repeated, for the whole sample, with a larger erosion depth. The final result of the particle detection is shown in Fig. 2f.

The sizes, positions and orientations of the ellipsoids can be extracted from the volume, centers of mass and the moment tensors $W_0^{2,0} = \int_{\text{grain}} \vec{r} \otimes \vec{r}\ \mathrm{d}V$ (similar to the tensor of inertia) where $\vec{r}$ is the position vector [18] of the labelled clusters.

Contact Numbers

The local contact number of a given grain is the number of other grains with which it is in geometric (point) contact. For experimental data, the contact numbers are hard to determine, because the contact number depends on the exact particle positions and their orientations. The finite accuracy of the X-Ray tomography and the reconstruction as well as deviations of experimental particle shape from perfect ellipsoids lead to small deviations in position and orientations. Hence, a simple geometric "contact counting" would lead to incorrect or at least very noise-sensitive estimates of the contact number. The polydispersity of the particles does not affect the determination of the contact number, because the analysis presented here treats the ellipsoids as polydisperse objects.

To determine the average contact number of an ellipsoid ensemble, an algorithm is needed to decide whether two given ellipsoids are in touch or not. This can be formulated as a constrained minimization, which can be solved by the method of Lagrange multipliers [19] and Newton's method [14].

In order to extract the average contact number k from the tomographic data, the method introduced by Aste *et al.* for spheres [9] is improved and generalized for ellipsoids.

A morphological scaling factor of the ellipsoids x is introduced. The scaling factor x dilates the ellipsoids with a sphere B_s of radius s, where $s = x \cdot \sqrt[3]{\frac{3V_{av}}{4\pi}}$ and V_{av} is the average Volume of the ellipsoids in the ensemble. A negative x leads to an erosion of the ellipsoids. An illustration can be seen in Fig. 3.

The average contact number of an ellipsoid ensemble can be extracted from a *contact number scaling function* (CNS function). The CNS function maps the morphological scaling factor x onto the average contact number of the ensemble. The CNS function is a sum of two parts $f_1(x)$ and $f_2(x)$.

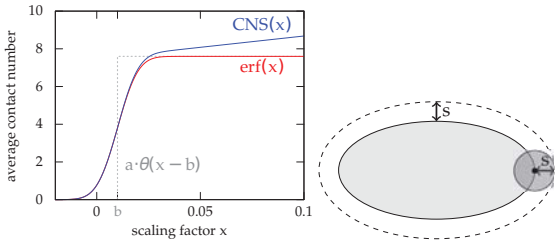

FIGURE 3. (left) Model of the fitted contact number scaling (CNS) function to extract the average contact number from tomographic data; (blue) CNS function, (red) error function, (dashed) step function. (right) Morphological dilation of the ellipsoids by a sphere of radius s.

The first part of this sum $f_1(x)$ is represented by a step function convoluted with a Gauss function. To understand this part, exact data of jammed hard ellipsoids is assumed where no ellipsoids overlap and each ellipsoid touches its neighbors at one single point. In this case, if the dilated ellipsoids are smaller than their actual size (for $x < b$) there should be no contacts. When the ellipsoids reach their actual size (for $x = b$), the function jumps to the average contact number a of the ensemble. The morphological scaling factor at this point is denoted by b. Hence, for exact data the first part of the CNS function can be described by a step function $h(x)$. (The second part of the sum $f_2(x)$, relevant for the gradually increasing number of contact when the ellipsoids are dilated beyond their original size for $x > b$, is dealt with below).

For experimental data, the position, size and orientation of the ellipsoids are not exact. These errors are assumed to be represented by the Gauss function

$$g(x) = \frac{c}{\sqrt{\pi}} \mathrm{e}^{-(c\cdot x)^2} \quad , \quad \sigma = \frac{1}{\sqrt{2}c} \tag{1}$$

with width σ.
The first summand of the CNS function for experimental data can be calculated as the convolution of the step function $h(x)$ and the Gauss function $g(x)$:

$$f_1(x) = h(x) * g(x) = \frac{a}{2} + \frac{a}{2} \operatorname{erf}(c\,(x-b)) \tag{2}$$

with the error function $\operatorname{erf}(x) = \frac{2}{\sqrt{\pi}} \int_0^x \mathrm{e}^{-\tau^2} \mathrm{d}\tau$.

When the ellipsoids are dilated beyond their original size ($x > b$), ellipsoids which have no physical contact but are close to each other develop contact points. This increase of the CNS function with x is, by lack of deeper insight, assumed to be a linear function $f_2(x)$ with slope d. The function $f_2(x)$ starts at the inflection point of the error function, and is defined by:

$$f_2(x) = \theta(x-b) \cdot d \cdot (x-b) \tag{3}$$

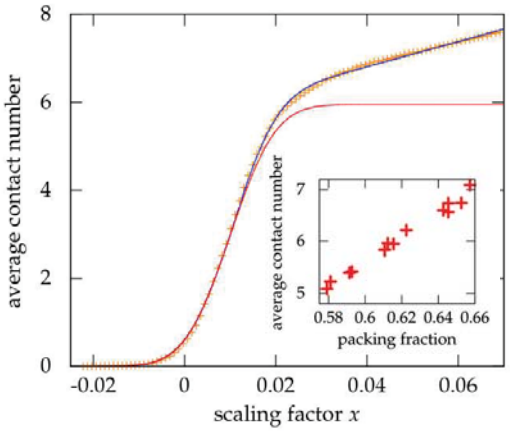

FIGURE 4. Fit of the CNS function (blue) to the tomographic data (orange crosses). The inset shows the average contact number as a function of the global packing fraction for oblate ellipsoids with an aspect ratio of 0.80.

The size of the ellipsoids at the inflection point b is the actual size of the ellipsoids.

The combined CNS function for the analysis of the tomographic data is the sum of the convolution of $h(x)$ and $g(x)$ (equation (2)) and the linear increase $f_2(x)$:

$$\mathrm{CNS}(x) = \frac{a}{2}\Big(1+\mathrm{erf}\big(c\,(x-b)\big)\Big) + \theta(x-b)\cdot d\cdot(x-b) \tag{4}$$

An illustration of the CNS function can be seen in Fig. 3.

The parameters of the CNS function can be tuned to match the discrete CNS function which can be extracted of the detected ellipsoids in a tomographic image. We fit the CNS function to the data of the detected ellipsoids, see Fig. 4. Finally, the fit parameter a represents the average contact number of the data set.

The width of the error function σ is a good indicator for the accuracy of the particle shapes. It is obvious that the larger σ, the larger the ambiguity of the exact value of the average contact number.

Beyond its use to determine average contact numbers, the CNS function can also be used to determine the size of the ellipsoids in the tomographic data, even if particles are polydisperse. For calculating the packing fraction, the ellipsoids are dilated to their actual size indicated by the inflection point of the CNS function.

For each jammed ellipsoid configuration the average contact number can be determined with this method. The contact numbers are only calculated in the middle of the container, excluding the outermost layers. Ellipsoids closer than 2 cm to the container wall are ignored to reduce boundary effects. The inset in Fig. 4 shows the average contact number as a function of the global packing fraction for packings of different global packing fractions of oblate ellipsoids (axis lengths $c:c:a$) with aspect ratio $c/a = 0.80$. The average contact numbers as a function of the global packing fraction collapse to one line.

CONCLUSIONS

The determination of contact numbers by the contact number scaling function approach seems to be feasible for disordered packings of ellipsoids, imaged by tomography. This tool can be applied to gain a better understanding of structure and mechanical stability of packings of aspherical particles.

ACKNOWLEDGMENTS

We thank Tim Senden for producing ellipsoids by 3D printing and Sebastian Kapfer for useful discussions. We acknowledge funding by the German Science Foundation (DFG) through the research group "Geometry and Physics of Spatial Random Structures" under grant no SCHR-1148/3-1.

REFERENCES

1. S. Torquato, and F. H. Stillinger, *Rev. Mod. Phys.* **82**, 2633–2672 (2010).
2. A. Donev *et. al*, *Science* **303**, 990–993 (2004).
3. A. Donev, R. Connelly, F. H. Stillinger, and S. Torquato, *Phys. Rev. E* **75**, 051304 (2007).
4. G. W. Delaney, and P. W. Cleary, *EPL* **89**, 34002 (2010).
5. G. W. Delaney, J. E. Hilton, and P. W. Cleary, *Phys. Rev. E* **83**, 051305 (2011).
6. S. C. Kapfer, W. Mickel, K. Mecke, and G. E. Schröder-Turk, *Phys. Rev. E* **85**, 030301 (2012).
7. C. Radin, *J. Stat. Phys.* **131**, 567–573 (2008).
8. Y. Jin, and H. A. Makse, *Phys. A* **389**, 5362 – 5379 (2010).
9. T. Aste, M. Saadatfar, and T. J. Senden, *Phys. Rev. E* **71**, 061302 (2005).
10. M. Neudecker, S. Ulrich, S. Herminghaus, and M. Schröter, *ArXiv e-prints* (2012), 1202.6272.
11. J. D. Bernal, and J. Mason, *Nature* **188** (1960).
12. L. E. Silbert, D. Ertaş, G. S. Grest, T. C. Halsey, and D. Levine, *Phys. Rev. E* **65**, 031304 (2002).
13. M. Saadatfar, A. N. P. Shepard, and M. K. A. Knackstedt, *Grain Partitioning and its Applications*, ISTE, 2010, pp. 269–276.
14. W. Press, S. Teukolsky, W. Vetterling, and B. Flannery, *Numerical Recipes, The Art of Scientific Computing*, Cambridge University Press, 2007, 3 edn.
15. P. Soille, *Morphological Image Analysis: Principles and Applications*, Springer-Verlag New York, Inc., 2003.
16. Ingemar, and Ragnemalm, *Pattern Recogn. Lett.* **13**, 161 – 166 (1992).
17. P. Felzenszwalb, and D. Huttenlocher, Distance transforms of sampled functions, Tech. rep. (2004).
18. G. E. Schröder-Turk *et. al*, *Adv. Mater.* **23**, 2535–2553 (2011).
19. P. J. Schneider, and D. Eberly, *Geometric Tools for Computer Graphics*, Elsevier Science Inc., New York, NY, USA, 2002.